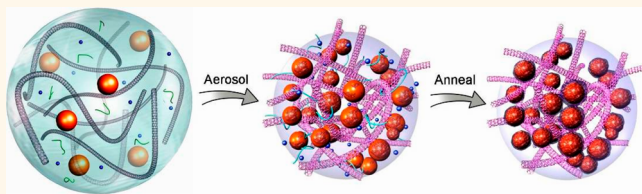


Building Robust Carbon Nanotube-Interweaved-Nanocrystal Architecture for High-Performance Anode Materials

Xilai Jia,^{†,‡} Yanhua Cheng,[§] Yunfeng Lu,^{*,§} and Fei Wei^{*,†}

[†]Beijing Key Laboratory of Green Chemical Reaction Engineering and Technology, Department of Chemical Engineering, Tsinghua University, Beijing 100084, People's Republic of China, [‡]State Key Laboratory of Heavy Oil Processing, China University of Petroleum, Changping, Beijing 102249, People's Republic of China, and [§]Department of Chemical and Biomolecular Engineering, University of California, Los Angeles, California 90095, United States

ABSTRACT Rational design of electrode materials is essential but still a challenge for lithium-ion batteries. Herein, we report the design and fabrication of a class of nanocomposite architecture featured by hierarchically structured composite particles that are built from iron oxide nanocrystals and carbon nanotubes. An aerosol spray drying process was used to synthesize this architecture. Such nanoarchitecture enhanced the ion transport and conductivity that are required for high-power anodes. The large volume changes of the anodes during lithium insertion and extraction are accommodated by the particle's resilience and internal porosity. High reversible capacities, excellent rate capability, and stable performance are attained. The synthesis process is simple and broadly applicable, providing a general approach toward high-performance energy storage materials.



KEYWORDS: lithium-ion battery · carbon nanotube · nanostructured composite · aerosol spray drying

The development of electrochemical energy storage devices with high energy density, power density, and cycling stability is of great importance for electronics, vehicles, large-scale power-grid storage, and other applications.^{1–3} In this context, lithium-ion batteries are of particular promise because their rate capability and cycling stability could be further improved. To achieve this goal, such devices must possess robust and effective enough transport networks for ions and electrons. However, most active materials used to date generally possess low electron conductivity and ion mobility. To construct the conducting networks, particles of active materials often with low-dimensional structures, conducting agents (e.g., carbon blacks), and polymeric binders are mixed and coated on current collectors. Such binder-holding structures, however, are easily destroyed particularly for high-capacity materials with large volume change during lithium insertion and extraction.^{4,5} Moreover, accompanying electrochemical reactions, electrically insulated solid electrolyte interphases (SEI) may be formed around the active material

particles and isolate the particles from their conductive networks, further resulting in capacity fading and deteriorated rate capability.⁶

To address these challenges, much effort has been devoted to constructing robust networks for effective transport of electrons and ions, such as coating the active materials with conductive coating (typically carbons),^{7,8} loading the active materials within porous conductive scaffolds,^{9,10} and forming the nanocomposites with sp^2 -hybridized carbons (e.g., carbon nanotubes (CNTs) and graphene).^{11–15} The nanocomposite strategy is particularly promising since it may provide long-range conductivity, better-controlled interface between the active materials and the conducting carbons, and more robust network structure.

To date, various nanocomposites have been prepared mainly by growing or assembling active materials (e.g., nanoparticles, nanorods, nanowires, and nanosheets) onto CNT networks,^{16,17} graphene sheets,^{18,19} or CNT–graphene composites.²⁰ Current CNT-based composites mainly include three categories: (i) the coaxial structures with

* Address correspondence to wf-dce@tsinghua.edu.cn, liucla@ucla.edu.

Received for review June 10, 2014 and accepted August 29, 2014.

Published online August 29, 2014
10.1021/nn5031302

© 2014 American Chemical Society

active materials coated on CNTs;^{21,22} (ii) the interpenetrating structures with active nanorods or nanowires intertwining within networks of CNT;^{23,24} and (iii) the integrated structure made from active materials and threading CNT networks.²⁵ The first category of composites facilitates effective charge transfer locally; however, it precludes the long-range conductivity since the active layer increases CNT contact resistance. For the second category of composites, interpenetrating structure provides porous networks and better conductivity throughout the whole electrodes; however, such composites suffer from loose interfacial contact and low structural integrity. As for the third category of composites, they usually show intimate interfacial contacts and robust structural integrity, thus offering better electrode performance. Herein, we report the method of making CNT nanocomposites with integrated structure by a simple spray drying process as high-performance anode materials. Fe_3O_4 was used as a model material because of its wide applications in energy storage.

Exemplified using the synthesis of anode nanocomposites, Scheme 1 illustrates our synthesis approach. First, oxide nanocrystals (NCs) (e.g., as-prepared Fe_3O_4) and multiwalled CNTs after purification,²⁶ together with sucrose, were dispersed into aqueous solution assisted by a surfactant (P123, $\text{EO}_{20}\text{PO}_{70}\text{EO}_{20}$, where EO and PO are ethylene oxide and propylene oxide, respectively). Atomization of such colloidal dispersion generated aerosol droplets (Scheme 1A) passing through a heated tube furnace. Solvent evaporation from these droplets condensed the nonvolatile components upon

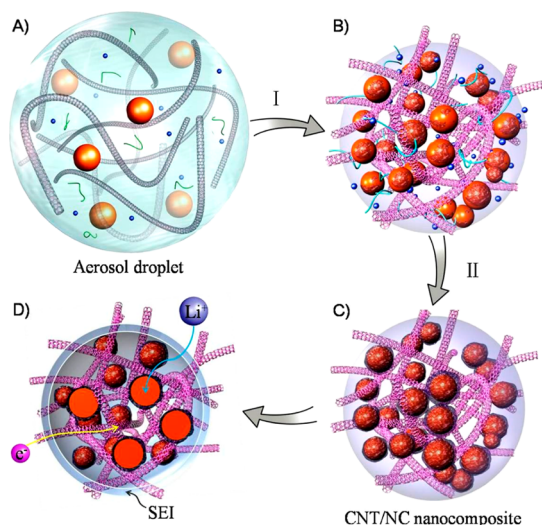
drying (step I), forming composite particles (Scheme 1B) that were collected in a filter. Subsequent annealing process (step II) led to the formation of nanocomposite particles (Scheme 1C) with robust and effective networks for electron and ion transport.

During the spraying process, CNTs and NCs were confined and closely packed within the droplets, forming spherical particles threaded by CNTs. The annealing process further sintered the NCs, forming continuous NC networks. At the same time, the sucrose was converted into carbon coating for the NCs and solidified the interface between the CNTs and NCs. Such structure offers shortened solid-phase ion diffusion length and excellent conductivity within the particles. The CNTs extruded out of the nanocomposite particles provide long-range conductivity through intraparticle contacts of such CNTs. Besides the improved ion and electron conductivity, such nanocomposite architecture also effectively circumvents the issues associated with the SEI formation. As depicted in Scheme 1D, during the initial charging and discharging cycles, although insulated SEI layers may be formed around the particles, the CNTs threading through the particles and extending out of the particles can still transfer electrons effectively by crossing the SEI layers. In short, this architecture provides the nanocomposites with robust pathways for ion and electron transport, enabling the fabrication of high-performance electrodes. It is also important to mention that the spraying process is facile and scalable for industrial processes,^{27–30} and adapting such a scalable process allows the production of high-performance electrode materials at low cost.

RESULTS AND DISCUSSION

Figure 1A shows a representative scanning electron microscope (SEM) image of the nanocomposite particles. The particle morphology is rough, with threading CNTs visible on the surfaces. The nanocomposites are spherical granules with polydisperse submicron sizes (Figure 1B) ranging from ~ 0.3 to $0.6 \mu\text{m}$. Those assembled composite particles can circumvent the limitation of low-dimensional nanoparticles and offer easier handling.³¹ Close observation of transmission electron microscopy (TEM, Figure 1C) confirms that the composite particles are made from networks of Fe_3O_4 NCs and CNTs threading through the particles. Moreover, the Fe_3O_4 networks are coated by decomposed carbons and connected with CNTs (Figure 1D), forming three-dimensional (3D) long-range conductive networks throughout the whole particles. The elemental mapping of the composite particles was obtained by energy-dispersive X-ray spectroscopy (EDS, Figure 1E), which further confirmed the uniform distribution of Fe_3O_4 within the 3D carbon networks.

X-ray powder diffraction (XRD) pattern (Figure 2A) shows that the Fe_3O_4 NCs in the composites were



Scheme 1. Schematic fabrication of CNT/NC nanocomposites through an (I) aerosol spray drying process followed by (II) thermal annealing. (A) The droplets generated by the aerosol process are condensed into (B) solidified particles after passing through a heated furnace and then are converted into (C) the nanocomposites consisting of NCs and threading CNTs after further annealing. (D) Formation of SEI protection on the nanocomposites during the initial charge/discharge cycles.

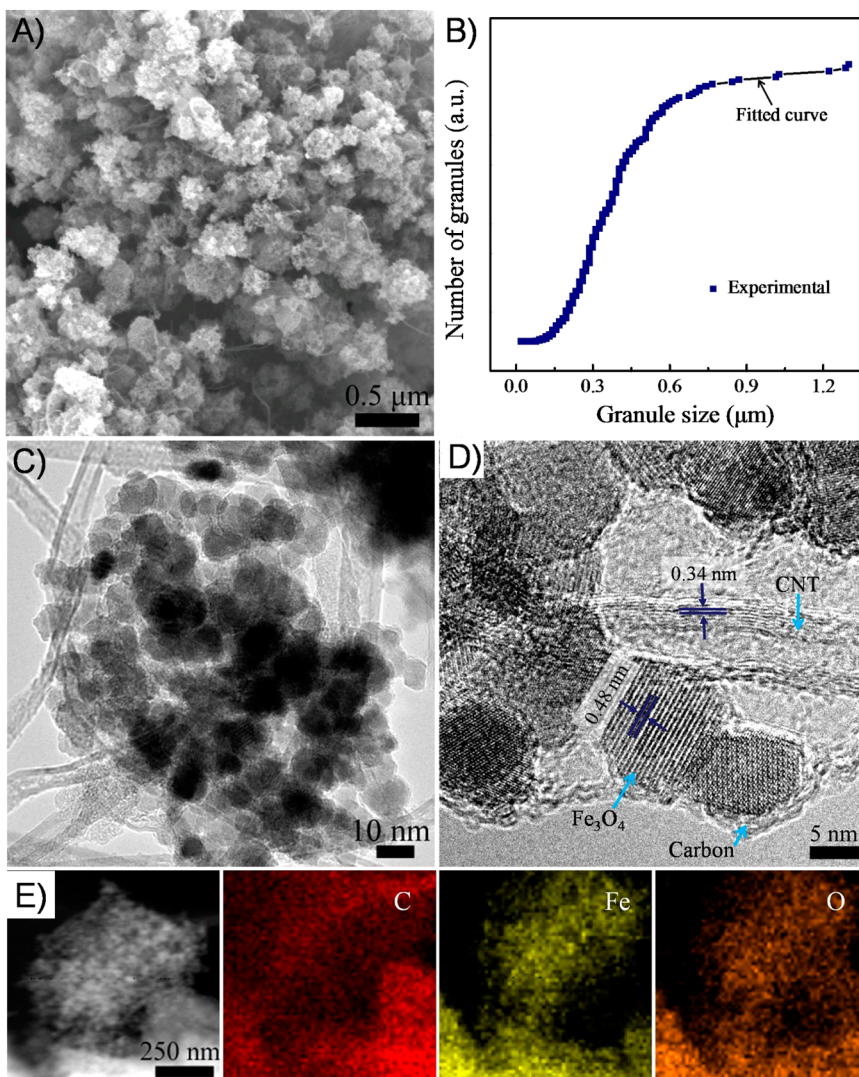


Figure 1. (A) SEM image of CNT/Fe₃O₄ nanocomposites. (B) Cumulative size distribution of the spherical composite granules. (C) TEM image showing interwoven networks. (D) High-resolution TEM micrograph of the nanocomposites. (E) STEM image of CNT/Fe₃O₄ nanocomposites and the corresponding elemental mapping images of C (red), Fe (green), and O (orange).

calculated to be 9.3 nm from the Scherrer equation, which minimizes sluggish solid-state ion transport due to the low dimensionality. Heating CNT/Fe₃O₄ nanocomposites in nitrogen at 560 °C completely decomposed residual surfactants and converted sucrose into carbons, which strongly cross-linked the interfaces of CNTs and Fe₃O₄ networks. We noticed that such a heating treatment did not lead to size growth of Fe₃O₄ NCs because they were encapsulated by decomposed carbon coating. Raman spectra (Figure 2B) reveal that the carbons in the composites have high graphitization due to the introduction of sp²-hybridized CNTs. Characteristic peaks of the D and G bands corresponding to the disordered and graphitized carbons were observed at 1334 and 1596 cm⁻¹, respectively. The element composition (84 wt % Fe₃O₄, 16 wt % C) was calculated by thermogravimetric analysis (TGA, Figure 2C), suggesting a high active material loading. In addition, interconnected porous channels existed in the composites.

Consequently, nitrogen adsorption–desorption isotherms (Figure 2D) of the nanocomposite particles suggest a high Brunauer–Emmett–Teller (BET) surface area of 95.8 m² g⁻¹ and hierarchically structured pores (inset of Figure 2D) for fast electrolyte transport.

Apart from the aforementioned structural features, CNT/Fe₃O₄ nanocomposite particles also show mechanical robustness. The compression–resilience properties of the nanocomposites are compared with bare Fe₃O₄ NCs and aerosol-synthesized Fe₃O₄/carbon nanocomposites³² without CNTs using cycled compression (Figure 3A). It suggests that CNT/Fe₃O₄ composite particles have elastic properties to cushion volume changes due to the introduction of CNTs. More specifically, CNT/Fe₃O₄ composite particles allow large compressive strain (e.g., >32%) yet possess the ability of shape recovery. In contrast, despite a low compressive strain of ca. 6%, Fe₃O₄/carbon composite particles show limited recovery ability (left inset of Figure 3A),

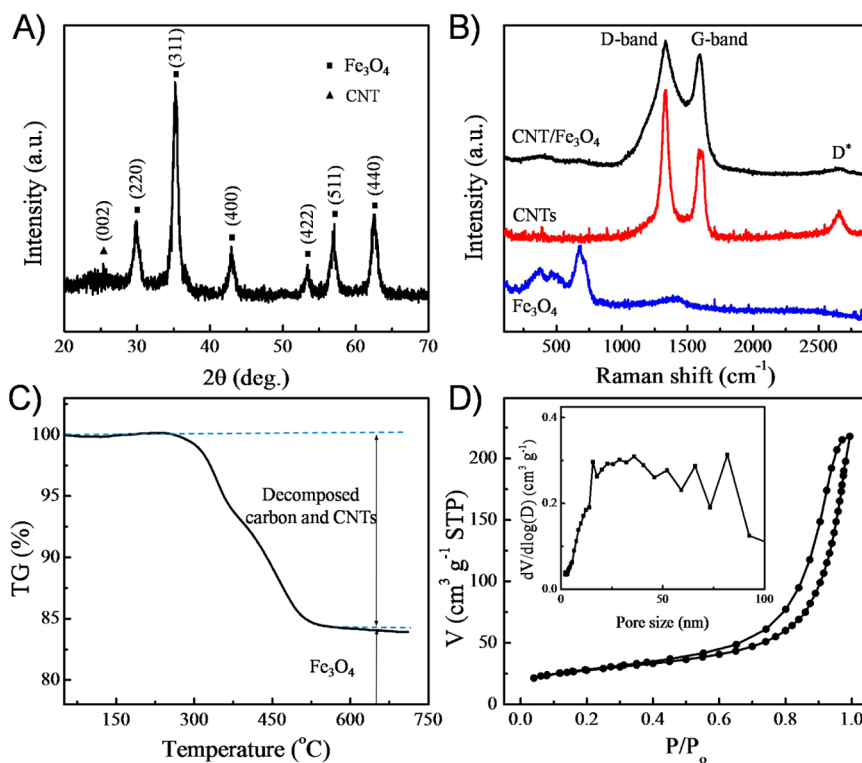


Figure 2. (A) XRD pattern of CNT/Fe₃O₄ nanocomposites after thermal annealing. (B) Raman spectra of CNT/Fe₃O₄ nanocomposites, CNTs, and Fe₃O₄ NCs. (C) TGA curve of CNT/Fe₃O₄ composite particles. (D) N₂ sorption isotherms and Barrett–Joyner–Halenda pore size distribution (inset) of CNT/Fe₃O₄ nanocomposites.

whereas bare Fe₃O₄ NCs nearly lose all their recovery ability (right inset of Figure 3A). The volume conductivity of CNT/Fe₃O₄ particles without pressure was $\sim 4 \times 10^{-3}$ S m⁻¹ (Figure 3B), more than 1000 times higher than that of aerosol-synthesized Fe₃O₄/carbon particles, suggesting the significant improvement of electron transport. When compressed, CNT/Fe₃O₄ composites with an increased conductivity appeared at 38% strain, much larger than that of Fe₃O₄/carbon composite particles ($\sim 7\%$). This phenomenon suggested that a hierarchical structure existed in the nanocomposites.³³ Therefore, elastic conductive networks and interconnected pores were synergistically constructed in CNT/Fe₃O₄ nanocomposites with structure durability. Despite other crystalline particles and graphene oxide that were used to synthesize their composites using this technique,^{34,35} this contribution was the first demonstration of nanocomposites based on CNTs and NC building blocks and enriched high-performance nanostructures for energy storage.

As a proof of concept, we measured the electrochemical performance of the CNT/Fe₃O₄ nanocomposites as anode materials for Li-ion batteries. Charge storage behavior of the nanocomposites was characterized by cyclic voltammetry (CV) at 0.2 mV s⁻¹ (Figure 4A). In the first cycle, an irreversible capacity loss at 0.63 V was observed, corresponding to the irreversible reduction of electrolyte and SEI formation, as discussed.¹⁶ Then, a slight shift of the CV curves was observed.

Redox reactions of lithium insertion/extraction were highly reversible in the subsequent cycles, where the anodic Li extraction occurred at 0.77 V and the cathodic Li insertion occurred around 1.7 V. Figure 4B shows the galvanostatic charge/discharge curves of the CNT/Fe₃O₄ electrode at various rates. The initial charge and discharge capacities of the total anode at a current density of 72 mA g⁻¹ were 1372.9 and 893.2 mAh g⁻¹ respectively, offering a modest initial Coulombic efficiency of 65%. Moreover, charge–discharge curves of the electrode at increasing current densities show that the reaction kinetics was well maintained due to the hierarchical structure of the nanocomposites and, more importantly, increased conductivity. The capacity contribution of CNTs within the nanocomposite electrode was relatively small compared to that of Fe₃O₄ at a voltage of 0.005–3.0 V (Supporting Information Figure S1). When the CNT contribution was deducted, the Fe₃O₄ component in the electrode displayed a discharge capacity of ~ 1210 mAh g⁻¹ at 72 mA g⁻¹, which is higher or comparable to those of reported iron oxide anodes.^{7,36–38}

Whereas metal oxides are known to suffer from sluggish kinetics, the designed CNT/Fe₃O₄ nanocomposites demonstrate excellent rate capability. In Figure 4C, an averaged discharge capacity of 984 mAh g⁻¹ was realized based on the whole mass of an electrode at 0.1 C (1 C = 720 mA g⁻¹ based on the total mass of the electrode, including CNT/Fe₃O₄ composite particles,

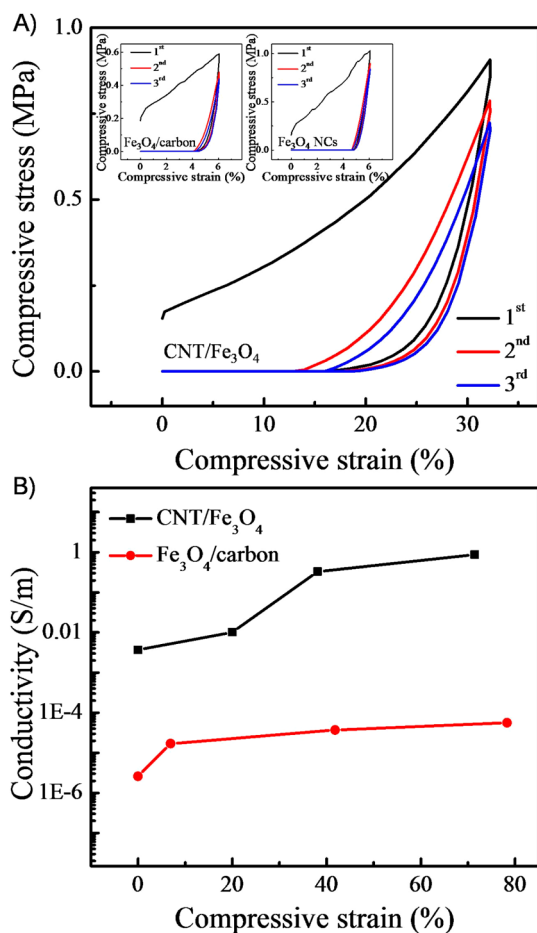


Figure 3. (A) Compressive stress–strain curves of CNT/Fe₃O₄ nanocomposites in comparison with that of CNT/carbon nanocomposites (left inset) and pure Fe₃O₄ NCs (right inset). (B) Volume conductivity of CNT/Fe₃O₄ and Fe₃O₄/carbon composite particles with increasing compressive strain.

polyvinylidene fluoride (PVDF), and conductive agents). When current densities increased, little decrease of capacity was observed before the 1 C rate. Even at high current rates, such as 12 C, the electrode retained a capacity of 440 mA h g⁻¹, still exceeding graphite's theoretical capacity. Such electrode rate capability performance exceeded most reported iron-oxide-based electrodes,^{39–46} and other oxide anode materials.^{47–50} Moreover, aerosol-synthesized Fe₃O₄/carbon composite particles were also prepared as anode materials. It showed that the Fe₃O₄/carbon electrode reached similar capacity at low rates (before 1 C); however, the performance deteriorated at high rates, which confirmed better electron transport of CNT/Fe₃O₄ composites. The aerosol-synthesized CNT/Fe₃O₄ and Fe₃O₄/carbon composite electrodes performed much better than bare Fe₃O₄ electrode, suggesting robust kinetics of the self-assembled composites using the aerosol spray technique.

Based on the robust structure features, CNT/Fe₃O₄ nanocomposites offer remarkable cycling stability. As shown in Figure 4D, the composite electrode offered

a total discharge capacity of ~900 mA h g⁻¹ at 1 C in the initial cycles and was gradually maintained at ~1000 mA h g⁻¹ without obvious capacity fading during 100 cycles. The capacity increase with cycling was observed in various nanostructured metal oxide electrodes.^{51,52} The activation of active materials and some reversible formation of polymeric/gel-like deposition of electrolyte have been suggested as possible reasons.²² Coulombic efficiency was maintained around 98% from the second cycle (Supporting Information Figure S2), supporting the highly reversible electrochemical reaction upon cycling. In comparison, aerosol-synthesized Fe₃O₄/carbon composites offered limited stability, and it gradually faded after ~50 cycles. Based on the mechanical properties of CNT/Fe₃O₄ nanocomposites, it was suggested that the effect of repeated volume changes on cycling performance was mitigated by the elastic properties. As for the bare Fe₃O₄ electrode, it could hardly offer stable performance. The capacity faded to less than 300 mA g⁻¹ after 50 cycles. Clearly, CNT/NC nanocomposites show outstanding performance as long-lifetime electrode materials.

To understand the reason for the high stability, electrochemical impedance spectroscopy (EIS) was conducted on CNT/Fe₃O₄ composite electrodes upon their charge/discharge cycling (Figure 5A). The Nyquist plots at different cycles (e.g., fresh electrode, the sixth, and 101st cycles) display similar intercepts (around 2.0 Ω) that represent ohmic resistance from the contact, electrode, and resistance from the electrolyte. With frequency decreases, the electrode exhibits a semicircle due to the charge transfer resistance between the electrode and the electrolyte. There was a slight decrease in semicircle diameter at the sixth cycle, indicating excellent electrode stability with an activation process. The diameter of the semicircle increased in the following cycles and after 100 cycles; accordingly, the charge transfer resistance increased from 30 to 140 Ω, which was associated with forming SEI. The following sloping region after the semicircle in the low-frequency region reflects the diffusion resistance of the electrolyte ions into the electrode. Obviously, the ion transport pathway was well maintained during cycling, indicated by the similar features of the subvertical profiles. The results indicated that the electron conduction and ion diffusion pathways in the composite electrodes were well maintained despite SEI formation during charge/discharge cycles.

To further confirm the robust structure, the morphology of CNT/Fe₃O₄ composite particles in the initial lithiated electrode (electrode discharged to 0.005 V) and the electrode cycled after 100 cycles was examined under electron microscopes. Indeed, the composites retained their spherical interwoven structure at the initial discharge state (Supporting Information Figure S3). Even after the long-term cycling, it shows

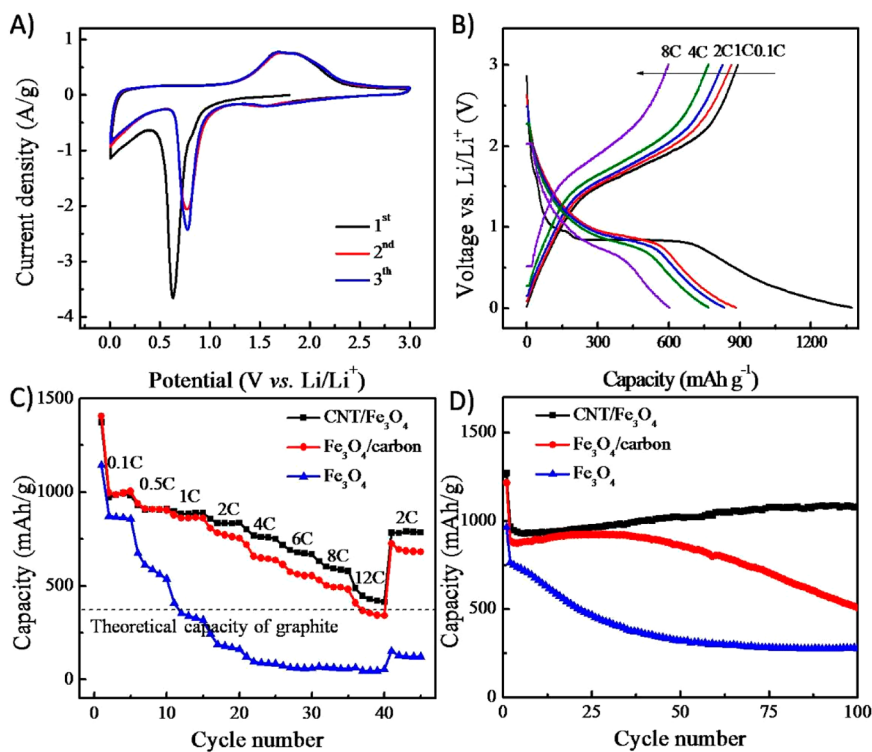


Figure 4. Electrochemical performance of CNT/Fe₃O₄ nanocomposites as anode materials. (A) CV curves of a CNT/Fe₃O₄ electrode collected at a scan rate of 0.2 mV s⁻¹. (B) Charge–discharge curves of a CNT/Fe₃O₄ electrode at various rates in the potential window of 0.005–3.0 V. (C) Rate capability comparison of CNT/Fe₃O₄, Fe₃O₄/carbon, and bare Fe₃O₄ electrodes. (D) Cycling stability of a CNT/Fe₃O₄ electrode in comparison with that of Fe₃O₄/carbon and bare Fe₃O₄ electrodes at a rate of 1 C.

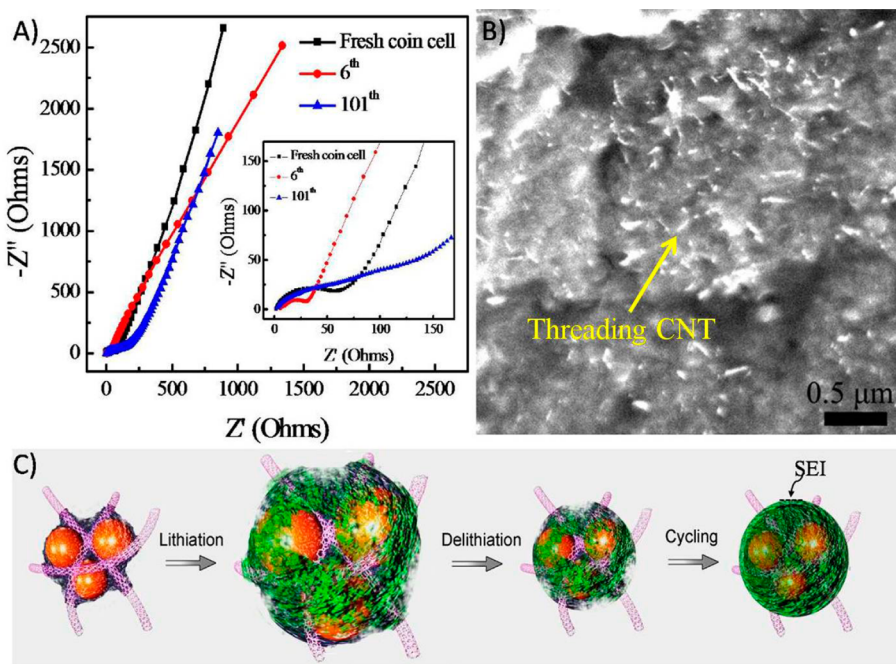


Figure 5. (A) Electrochemical impedance spectra of a CNT/Fe₃O₄ nanocomposite electrode at fresh half-coin cell, sixth, and 101st cycles over the frequency range of 10⁵ to 0.01 Hz. (B) SEM image of CNT/Fe₃O₄ spherical composite particles after 100 cycles. (C) Schematic of SEI formation in CNT/Fe₃O₄ nanocomposites upon cycling.

that the spherical structure was still maintained (Figure 5B). A polymer/gel-like coating that can be ascribed to SEI formation surrounds the composite

particles (Supporting Information Figure S4). To date, no effective methods can fully solve the problems caused by insulated SEI; however, the designed

nanocomposites successfully circumvent this problem compared to active particles coated by pyrolytic carbons or other coatings.^{53,54} Figure 5C is the schematic of interwoven structure evolution upon cycling. The robust structure allowed the composites to expand freely without mechanical failure during repeated lithiation. Therefore, despite SEI formation, threading CNTs of the composites could still transfer electrons effectively by crossing SEI throughout the whole composite particles. In this case, the SEI formation was transformed into a robust protection that promoted the structural integrity of the nanocomposite particles upon cycling. Then, robust performance was achieved in such nanocomposites.

CONCLUSION

In summary, we have demonstrated the synthesis of hierarchically nanostructured CNT-interweaved-nanocrystal architecture using an aerosol spray drying process for lithium battery anodes that yield high electrochemical performances. The nanoarchitecture exhibited effective electron and ion transport and, more importantly, mechanical robustness, thus endowing the battery electrodes with high reversible capacity and stable performance. This synthesis process is effective and can be readily extended to assemble CNTs with other functional units, offering huge families of nanostructured materials for a broad spectrum of applications.

EXPERIMENTAL METHODS

Material Synthesis. Fe_3O_4 NCs were synthesized using a co-precipitation method.³² Multiwalled CNTs were purified and dried before use.²⁶ Then, 60 mg of CNTs, 1.5 g of P123, and 0.3 g of sucrose were dispersed into 150 g of 0.53 wt % Fe_3O_4 colloidal solution using a fluid shearing dispersion method (~ 2000 r/min, 30 min), forming a homogeneous dispersion. The dispersion was then sent through an atomizer using nitrogen as a carrier gas. The produced aerosol droplets passed through a glass tube heated at 450°C ; as-formed particles were collected using a filter. Then, the particles were further annealed at 560°C for 2 h under nitrogen, forming CNT/ Fe_3O_4 composite particles. For comparison, CNT/carbon composite particles were prepared using the same process without addition of CNTs as the control sample.

Material Characterizations. SEM experiments were conducted on a JEOL JSM-6700 FE-SEM. TEM experiments were conducted on a FEI T12 instrument operating at 120 kV. EDS analysis was performed on the Tecnai G² F20 instrument using an equipped EDAX apparatus. Nitrogen sorption isotherms were measured at 77 K with a Micromeritics ASAP 2020 analyzer. The specific surface areas (S_{BET}) were calculated by the BET method using the adsorption branch in a relative pressure range from 0.04 to 0.25. The pore size distributions (D_p) were derived from the adsorption branch of isotherms using the Barrett–Joyner–Halenda model. X-ray diffraction was conducted on a Panalytical X'Pert Pro X-ray powder diffractometer using $\text{Cu K}\alpha$ radiation ($\lambda = 1.54$ Å). Raman spectra were performed on a Horiba Jobin Yvon Lab RAMHR800 Raman spectrometer with He–Ne laser excitation at 633 nm. Thermogravimetric analysis was conducted on a TGA Q50 instrument at a ramping rate of $10^\circ\text{C min}^{-1}$ under an air flow. To measure the conductivity, the composite particles were loaded into an insulated hollow cylinder, with one end tightly sealed by using a solid copper cylinder and the other end using a mobile one. A precompression of 0.1 MPa was performed on the loaded particles. The particles were compressed at different strains and measured their voltage–current curves using Agilent B2902A. Then, the volume conductivities were calculated. Mechanical compression tests were conducted on INSTRON 5843. The particles were also precompressed to 0.1 MPa. Then, the compression tests were cycled for three times at a speed of 1 mm min^{-1} at room temperature.

Electrochemical Characterizations. To make CNT/ Fe_3O_4 electrodes, 75.3 wt % of aerosol-synthesized CNT/ Fe_3O_4 composite particles, 9.46 wt % of CNTs, 4.84 wt % of CB, and 10.4 wt % of PVDF were mixed in *N*-methyl pyrrolidone to form slurries. Then, the slurries were coated onto titanium substrates and dried at 300°C for 5 h under nitrogen. The mass loading of active materials was $\sim 1.2\text{ mg cm}^{-2}$ on each current collector. Identical steps were used to prepare Fe_3O_4 /carbon and bare Fe_3O_4

electrodes. For the electrochemical test, the electrodes were assembled into 2032-type coin cells. The electrolyte was a 1.0 M LiPF_6 in ethylene carbonate/diethyl carbonate (1:1 by volume), and lithium foils were used as both the counter and reference electrodes. The CV and EIS measurements were carried out on a Solartron 1860/1287 electrochemical interface. Coin cell assemblies were conducted in an argon-filled glovebox. The galvanostatic charge/discharge measurements were carried out by LAND CT2000 battery tester.

Conflict of Interest: The authors declare no competing financial interest.

Acknowledgment. This work was supported by National Basic Research Program of China (No. 2011CB932602), Natural Scientific Foundation of China (No. 21306102), Science Foundation of China University of Petroleum, Beijing (No. 2462013YJRC028), and was supported as part of the Molecularly Engineered Energy Materials, an Energy Frontier Research Center funded by the U.S. Department of Energy, Office of Science, Office of Basic Energy Sciences under award DE-SC001342. The authors acknowledge Ph.D. candidate Yuanyuan Shang and Prof. Anyuan Cao of Peking University for the mechanical tests.

Supporting Information Available: Supplementary TEM and electrochemical performance data are included. This material is available free of charge via the Internet at <http://pubs.acs.org>.

REFERENCES AND NOTES

- Guo, Y.-G.; Hu, J.-S.; Wan, L.-J. Nanostructured Materials for Electrochemical Energy Conversion and Storage Devices. *Adv. Mater.* **2008**, *20*, 2878–2887.
- Liu, J.; Cao, G.; Yang, Z.; Wang, D.; Dubois, D.; Zhou, X.; Graff, G. L.; Pederson, L. R.; Zhang, J. G. Oriented Nanostructures for Energy Conversion and Storage. *ChemSusChem* **2008**, *1*, 676–697.
- Liu, C.; Li, F.; Ma, L.-P.; Cheng, H.-M. Advanced Materials for Energy Storage. *Adv. Mater.* **2010**, *22*, E28–E62.
- Poizot, P.; Laruelle, S.; Gruegeon, S.; Dupont, L.; Tarascon, J. M. Nano-Sized Transition-Metal Oxides as Negative-Electrode Materials for Lithium-Ion Batteries. *Nature* **2000**, *407*, 496–499.
- Wang, C.; Wu, H.; Chen, Z.; McDowell, M. T.; Cui, Y.; Bao, Z. Self-Healing Chemistry Enables the Stable Operation of Silicon Microparticle Anodes for High-Energy Lithium-Ion Batteries. *Nat. Chem.* **2013**, *5*, 1042–1048.
- Zhang, S.; Ding, M. S.; Xu, K.; Allen, J.; Jow, T. R. Understanding Solid Electrolyte Interface Film Formation on Graphite Electrodes. *Electrochim. Solid-State Lett.* **2001**, *4*, A206–A208.

7. Zhang, W.-M.; Wu, X.-L.; Hu, J.-S.; Guo, Y.-G.; Wan, L.-J. Carbon Coated Fe_3O_4 Nanospindles as a Superior Anode Material for Lithium-Ion Batteries. *Adv. Funct. Mater.* **2008**, *18*, 3941–3946.
8. Jung, H.-G.; Jang, M. W.; Hassoun, J.; Sun, Y.-K.; Scrosati, B. A High-Rate Long-Life $\text{Li}_4\text{Ti}_5\text{O}_{12}/\text{Li}[\text{Ni}_{0.45}\text{Co}_{0.1}\text{Mn}_{1.45}]\text{O}_4$ Lithium-Ion Battery. *Nat. Commun.* **2011**, *2*, 516.
9. Wu, Y.; Wei, Y.; Wang, J.; Jiang, K.; Fan, S. Conformal Fe_3O_4 Sheath on Aligned Carbon Nanotube Scaffolds as High-Performance Anodes for Lithium Ion Batteries. *Nano Lett.* **2013**, *13*, 818–823.
10. Zhang, H.; Yu, X.; Braun, P. V. Three-Dimensional Bi-continuous Ultrafast-Charge and -Discharge Bulk Battery Electrodes. *Nat. Nanotechnol.* **2011**, *6*, 277–281.
11. Xin, S.; Guo, Y. G.; Wan, L. J. Nanocarbon Networks for Advanced Rechargeable Lithium Batteries. *Acc. Chem. Res.* **2012**, *45*, 1759–1769.
12. Liu, X.-M.; Zhang, B.; Ma, P.-C.; Yuen, M. M.; Kim, J.-K. Carbon Nanotube (CNT)-Based Composites as Electrode Material for Rechargeable Li-Ion Batteries: A Review. *Compos. Sci. Technol.* **2012**, *72*, 121–144.
13. Wang, H.; Dai, H. Strongly Coupled Inorganic-Nano-carbon Hybrid Materials for Energy Storage. *Chem. Soc. Rev.* **2013**, *42*, 3088–3113.
14. Wu, Z.-S.; Zhou, G.; Yin, L.-C.; Ren, W.; Li, F.; Cheng, H.-M. Graphene/Metal Oxide Composite Electrode Materials for Energy Storage. *Nano Energy* **2012**, *1*, 107–131.
15. Zhang, Q.; Huang, J. Q.; Qian, W. Z.; Zhang, Y. Y.; Wei, F. The Road for Nanomaterials Industry: A Review of Carbon Nanotube Production, Post-treatment, and Bulk Applications for Composites and Energy Storage. *Small* **2013**, *9*, 1237–1265.
16. Ban, C.; Wu, Z.; Gillaspie, D. T.; Chen, L.; Yan, Y.; Blackburn, J. L.; Dillon, A. C. Nanostructured Fe_3O_4 /SWNT Electrode: Binder-Free and High-Rate Li-Ion Anode. *Adv. Mater.* **2010**, *22*, E145–E149.
17. Jia, X.; Yan, C.; Chen, Z.; Wang, R.; Zhang, Q.; Guo, L.; Wei, F.; Lu, Y. Direct Growth of Flexible LiMn_2O_4 /CNT Lithium-Ion Cathodes. *Chem. Commun.* **2011**, *47*, 9669–9671.
18. Zhou, G.; Wang, D.-W.; Li, F.; Zhang, L.; Li, N.; Wu, Z.-S.; Wen, L.; Lu, G. Q.; Cheng, H.-M. Graphene-Wrapped Fe_3O_4 Anode Material with Improved Reversible Capacity and Cyclic Stability for Lithium Ion Batteries. *Chem. Mater.* **2010**, *22*, 5306–5313.
19. Wang, D.; Choi, D.; Li, J.; Yang, Z.; Nie, Z.; Kou, R.; Hu, D.; Wang, C.; Saraf, L. V.; Zhang, J. Self-Assembled TiO_2 –Graphene Hybrid Nanostructures for Enhanced Li-Ion Insertion. *ACS Nano* **2009**, *3*, 907–914.
20. Zhu, X.; Ning, G.; Fan, Z.; Gao, J.; Xu, C.; Qian, W.; Wei, F. One-Step Synthesis of a Graphene–Carbon Nanotube Hybrid Decorated by Magnetic Nanoparticles. *Carbon* **2012**, *50*, 2764–2771.
21. Liu, S.; Wang, Z.; Yu, C.; Wu, H. B.; Wang, G.; Dong, Q.; Qiu, J.; Eychmüller, A.; Lou, X. W. A Flexible TiO_2 (B)-Based Battery Electrode with Superior Power Rate and Ultralong Cycle Life. *Adv. Mater.* **2013**, *25*, 3462–3467.
22. Wang, Z.; Luan, D.; Madhavi, S.; Hu, Y.; Lou, X. W. D. Assembling Carbon-Coated $\alpha\text{-Fe}_2\text{O}_3$ Hollow Nanohorns on the CNT Backbone for Superior Lithium Storage Capability. *Energy Environ. Sci.* **2012**, *5*, 5252–5256.
23. Jia, X.; Chen, Z.; Suwarnasarn, A.; Rice, L.; Wang, X.; Sohn, H.; Zhang, Q.; Wu, B. M.; Wei, F.; Lu, Y. High-Performance Flexible Lithium-Ion Electrodes Based on Robust Network Architecture. *Energy Environ. Sci.* **2012**, *5*, 6845–6849.
24. Liu, B.; Wang, X.; Chen, H.; Wang, Z.; Chen, D.; Cheng, Y.-B.; Zhou, C.; Shen, G. Hierarchical Silicon Nanowires–Carbon Textiles Matrix as a Binder-Free Anode for High-Performance Advanced Lithium-Ion Batteries. *Sci. Rep.* **2013**, *3*, 1622.
25. Jia, X.; Zhang, L.; Zhang, R.; Lu, Y.; Wei, F. Carbon Nanotube-Penetrated Mesoporous V_2O_5 Microspheres as High-Performance Cathode Materials for Lithium-Ion Batteries. *RSC Adv.* **2014**, *4*, 21018–21022.
26. Jia, X.; Zhang, Q.; Zhao, M. Q.; Xu, G. H.; Huang, J. Q.; Qian, W.; Lu, Y.; Wei, F. Dramatic Enhancements in Toughness of Polyimide Nanocomposite via Long-CNT-Induced Long-Range Creep. *J. Mater. Chem.* **2012**, *22*, 7050–7056.
27. Boissiere, C.; Gross, D.; Chaumonnot, A.; Nicole, L.; Sanchez, C. Aerosol Route to Functional Nanostructured Inorganic and Hybrid Porous Materials. *Adv. Mater.* **2011**, *23*, 599–623.
28. Nandiyanto, A. B. D.; Okuyama, K. Progress in Developing Spray-Drying Methods for the Production of Controlled Morphology Particles: From the Nanometer to Submicrometer Size Ranges. *Adv. Powder Technol.* **2011**, *22*, 1–19.
29. Wang, C.; Wang, Y.; Graser, J.; Zhao, R.; Gao, F.; O'Connell, M. J. Solution-Based Carbohydrate Synthesis of Individual Solid, Hollow, and Porous Carbon Nanospheres Using Spray Pyrolysis. *ACS Nano* **2013**, *7*, 11156–11165.
30. Guo, J.; Liu, Q.; Wang, C.; Zachariah, M. R. Interdispersed Amorphous MnO_x –Carbon Nanocomposites with Superior Electrochemical Performance as Lithium-Storage Material. *Adv. Funct. Mater.* **2012**, *22*, 803–811.
31. Magasinski, A.; Dixon, P.; Hertzberg, B.; Kvit, A.; Ayala, J.; Yushin, G. High-Performance Lithium-Ion Anodes Using a Hierarchical Bottom-Up Approach. *Nat. Mater.* **2010**, *9*, 353–358.
32. Jia, X.; Chen, Z.; Cui, X.; Peng, Y.; Wang, X.; Wang, G.; Wei, F.; Lu, Y. Building Robust Architectures of Carbon and Metal Oxide Nanocrystals toward High-Performance Anodes for Lithium-Ion Batteries. *ACS Nano* **2012**, *6*, 9911–9919.
33. Liu, Y.; Qian, W.; Zhang, Q.; Cao, A.; Li, Z.; Zhou, W.; Ma, Y.; Wei, F. Hierarchical Agglomerates of Carbon Nanotubes as High-Pressure Cushions. *Nano Lett.* **2008**, *8*, 1323–1327.
34. Mao, S.; Wen, Z.; Kim, H.; Lu, G.; Hurley, P.; Chen, J. A General Approach to One-Pot Fabrication of Crumpled Graphene-Based Nanohybrids for Energy Applications. *ACS Nano* **2012**, *6*, 7505–7513.
35. Chen, Y.; Guo, F.; Jachak, A.; Kim, S. P.; Datta, D.; Liu, J.; Kulaots, I.; Vaslet, C.; Jang, H. D.; Huang, J. Aerosol Synthesis of Cargo-Filled Graphene Nanosacks. *Nano Lett.* **2012**, *12*, 1996.
36. Li, B.; Cao, H.; Shao, J.; Qu, M. Enhanced Anode Performances of The Fe_3O_4 -Carbon-rGO Three Dimensional Composite in Lithium Ion Batteries. *Chem. Commun.* **2011**, *47*, 10374–10376.
37. Geng, H.; Zhou, Q.; Pan, Y.; Gu, H.; Zheng, J. Preparation of Fluorine-Doped, Carbon-Encapsulated Hollow Fe_3O_4 Spheres as an Efficient Anode Material for Li-Ion Batteries. *Nanoscale* **2014**, *6*, 3889–3894.
38. He, C.; Wu, S.; Zhao, N.; Shi, C.; Liu, E.; Li, J. Carbon-Encapsulated Fe_3O_4 Nanoparticles as a High-Rate Lithium Ion Battery Anode Material. *ACS Nano* **2013**, *7*, 4459–4469.
39. Zhu, X.; Zhu, Y.; Murali, S.; Stoller, M. D.; Ruoff, R. S. Nanostructured Reduced Graphene Oxide/ Fe_2O_3 Composite as a High-Performance Anode Material for Lithium Ion Batteries. *ACS Nano* **2011**, *5*, 3333–3338.
40. Zhu, X.; Song, X.; Ma, X.; Ning, G. Enhanced Electrode Performance of Fe_2O_3 Nanoparticle-Decorated Nanomesh Graphene as Anodes for Lithium-Ion Batteries. *ACS Appl. Mater. Interfaces* **2014**, *6*, 7189–7197.
41. Zhang, F.; Zhang, T.; Yang, X.; Zhang, L.; Leng, K.; Huang, Y.; Chen, Y. A High-Performance Supercapacitor-Battery Hybrid Energy Storage Device Based on Graphene-Enhanced Electrode Materials with Ultrahigh Energy Density. *Energy Environ. Sci.* **2013**, *6*, 1623–1632.
42. Murali, T.; Murugan, A. V.; Manthiram, A. Facile Synthesis of Carbon-Decorated Single-Crystalline Fe_3O_4 Nanowires and Their Application as High Performance Anode in Lithium Ion Batteries. *Chem. Commun.* **2009**, *7360–7362*.
43. Yoon, T.; Chae, C.; Sun, Y.-K.; Zhao, X.; Kung, H. H.; Lee, J. K. Bottom-Up *In Situ* Formation of Fe_3O_4 Nanocrystals in a Porous Carbon Foam for Lithium-Ion Battery Anodes. *J. Mater. Chem.* **2011**, *21*, 17325–17330.
44. Bhuvaneswari, S.; Pratheeksha, P. M.; Anandan, S.; Rangappa, D.; Gopalan, R.; Rao, T. N. Efficient Reduced Graphene Oxide Grafted Porous Fe_3O_4 Composite as a High Performance Anode Material for Li-Ion Batteries. *Phys. Chem. Chem. Phys.* **2014**, *16*, 5284–5294.

45. Lee, S. H.; Yu, S.-H.; Lee, J. E.; Jin, A.; Lee, D. J.; Lee, N.; Jo, H.; Shin, K.; Ahn, T.-Y.; Kim, Y.-W.; Choe, H.; Sung, Y.-E.; Hyeon, T. Self-Assembled Fe_3O_4 Nanoparticle Clusters as High-Performance Anodes for Lithium Ion Batteries *via* Geometric Confinement. *Nano Lett.* **2013**, *13*, 4249–4256.
46. Chen, Y.; Song, B.; Lu, L.; Xue, J. Ultra-small Fe_3O_4 Nanoparticle Decorated Graphene Nanosheets with Superior Cyclic Performance and Rate Capability. *Nanoscale* **2013**, *5*, 6797–6803.
47. Paek, S.-M.; Yoo, E.; Honma, I. Enhanced Cyclic Performance and Lithium Storage Capacity of SnO_2 /Graphene Nanoporous Electrodes with Three-Dimensionally Delaminated Flexible Structure. *Nano Lett.* **2008**, *9*, 72–75.
48. Wang, H.; Cui, L.-F.; Yang, Y.; Sanchez Casalongue, H.; Robinson, J. T.; Liang, Y.; Cui, Y.; Dai, H. Mn_3O_4 -Graphene Hybrid as a High-Capacity Anode Material for Lithium Ion Batteries. *J. Am. Chem. Soc.* **2010**, *132*, 13978–13980.
49. Zhu, X.; Ning, G.; Ma, X.; Fan, Z.; Xu, C.; Gao, J.; Xu, C.; Wei, F. High Density Co_3O_4 Nanoparticles Confined in a Porous Graphene Nanomesh Network Driven by an Electrochemical Process: Ultra-high Capacity and Rate Performance for Lithium Ion Batteries. *J. Mater. Chem. A* **2013**, *1*, 14023–14030.
50. Ji, L.; Lin, Z.; Alcoutlabi, M.; Zhang, X. Recent Developments in Nanostructured Anode Materials for Rechargeable Lithium-Ion Batteries. *Energy Environ. Sci.* **2011**, *4*, 2682–2699.
51. Luo, J.; Liu, J.; Zeng, Z.; Ng, C. F.; Ma, L.; Zhang, H.; Lin, J.; Shen, Z.; Fan, H. J. Three-Dimensional Graphene Foam Supported Fe_3O_4 Lithium Battery Anodes with Long Cycle Life and High Rate Capability. *Nano Lett.* **2013**, *13*, 6136–6143.
52. Cheng, J.; Wang, B.; Park, C.-M.; Wu, Y.; Huang, H.; Nie, F. CNT@ Fe_3O_4 @C Coaxial Nanocables: One-Pot, Additive-Free Synthesis and Remarkable Lithium Storage Behavior. *Chem.—Eur. J.* **2013**, *19*, 9866–9874.
53. Sohn, H.; Chen, Z.; Jung, Y. S.; Xiao, Q.; Cai, M.; Wang, H.; Lu, Y. Robust Lithium-Ion Anodes Based on Nanocomposites of Iron Oxide-Carbon-Silicate. *J. Mater. Chem. A* **2013**, *1*, 4539–4545.
54. Li, H.; Wang, Z.; Chen, L.; Huang, X. Research on Advanced Materials for Li-Ion Batteries. *Adv. Mater.* **2009**, *21*, 4593–4607.